

# Measurement uncertainties in resonant characteristics of MEMS resonators<sup>†</sup>

Il Lee and Jungchul Lee\*

Department of Mechanical Engineering, Sogang University, Seoul, 121-742, Korea

(Manuscript Received June 18, 2012; Revised November 3, 2012; Accepted November 12, 2012)

## Abstract

This paper reports measurement of random uncertainties in resonant characteristics (resonance frequency and quality factor) of micro-electromechanical system (MEMS) resonators. We employ different methods to extract resonant characteristics of 4 different MEMS resonators which are either clamped-free or clamped-clamped beams. Each beam type operates either in air or in a partial vacuum, and therefore, different vacuum levels can be examined. Three different methods, including frequency sweep, impulse response, and thermal noise, are applied to each resonator type excited with electrostatic or piezo-crystal actuation. We make a thorough analysis and comparison for three different methods. Depending on device type and operating condition, there exists a better and recommended way to extract resonant characteristics of MEMS resonators. For example, the impulse response is best-suited for the quality factor measurement of a clamped-clamped beam operating in a vacuum. Our results show that the quality factor of MEMS resonators may be noticeably different and exhibit appreciable systematic and random uncertainties, and suggests a better way to extract the quality factor for a given situation.

*Keywords:* MEMS; Q-factor; Resonance frequency; Resonator; Uncertainty

## 1. Introduction

Many systems in engineering and physics exhibit resonant behaviors characterized with resonance frequency and quality factor (Q-factor). When a small excitation is applied, a given system oscillates with larger amplitude at resonance than at other frequencies since the system can store energy. Q-factor is defined as a ratio of the stored energy to the dissipated energy during one cycle operation. It is a dimensionless number which characterizes the quality of the given resonator. Such resonance phenomena occur in various systems including mechanical [1], acoustic [2-4], electrical [5], magnetic [6], optical [7, 8], and molecular systems [9]. Especially in micro-electromechanical systems (MEMS) resonators of our interest, both resonance frequency and Q-factor are popular research subjects [10]. For example, resonance frequency measurements have been exploited in mass sensing applications [11, 12], Q-factor measurements have been exploited in viscosity sensing [13, 14], and significant effort has been made towards Q-factor enhancement to improve the resonator performance [15, 16]. For such applications, it is prerequisite to make reliable and repeatable measurements on resonance frequency and Q-factor.

Resonance frequency and Q-factor of MEMS resonators can be measured with and without active actuation [17]. When

there is no active actuation, MEMS resonators are thermally vibrated and their noise spectra can be measured and analyzed to extract resonance frequency and Q-factor. This is often called passive method. With active actuation, MEMS resonators are subjected to either frequency sweep or impulsive drive input and measured amplitude or phase responses are analyzed accordingly. It is obvious that results from a passive method significantly depend on the performance of measurement systems used such as dynamic range, sampling rate, and resolution [18]. However, it is not straightforward to know whether results from active methods also mainly depend on the performance of measurement systems.

In different laboratories, the same types of resonators with similar geometries and under similar environmental conditions may be actuated differently. For example, electrostatic [19, 20], piezoelectric [21], thermomechanical [22, 23], or magnetic actuation [6, 24] are routinely employed. However, resonance frequency and Q-factor are often reported without specifying the actuation scheme. Unless the actuation modulates mechanical properties of resonators (for instance, periodic heating during thermomechanical actuation changes the elastic modulus of the resonator material [22]), it is reasonable to assume that resonance frequency is determined consistently regardless of the actuation scheme applied. But there is still no guarantee that damping is independent of actuation. Thus, it is interesting to know how much Q-factor varies with respect to the actuation scheme applied and to quantify measurement uncertainties. Recently, research efforts have been made to

\*Corresponding author. Tel.: +82 2 705 7973, Fax.: +82 2 712 0799

E-mail address: jayclee@sogang.ac.kr

<sup>†</sup>Recommended by Associate Editor Si-Hyung Lim

© KSME & Springer 2013

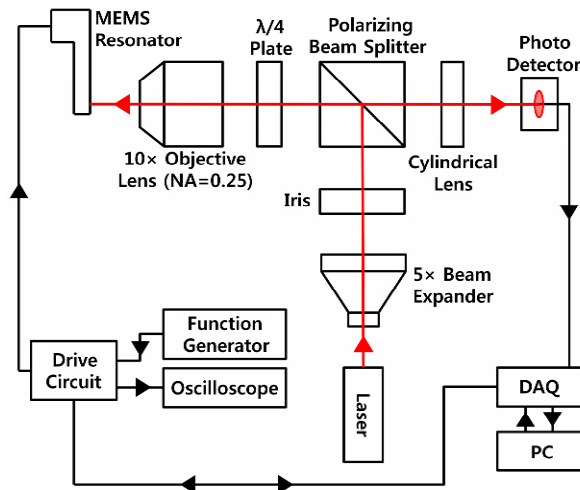


Fig. 1. Experimental setup used in this work. A polarized laser ( $d = 1\text{mm}$ ,  $\lambda = 633\text{nm}$ , and  $P = 5\text{mW}$ ) is expanded 5 times with a beam expander, goes through an iris, a polarizing beam splitter, a quarter wave ( $\lambda/4$ ) plate, then is focused onto a MEMS resonator with a  $10\times$  microscope objective ( $\text{NA} = 0.25$ ). The reflected light travels back to the polarizing beam splitter and is focused onto a two-segmented photodetector. The MEMS resonator is driven using a custom drive circuit in conjunction with a function generator or a data acquisition card. The photodetector output is monitored with an oscilloscope and recorded in a PC through the data acquisition card.

understand parameters or settings which possibly affect resonant characteristics of MEMS resonators including temperature [2, 25], pressure [25, 26], and actuation scheme [27]. However, detailed and thorough investigation regarding measurement uncertainties is still limited. Thus, it is necessary to specify measurement errors and to provide a guideline which suggests the best way to measure resonant characteristics precisely.

In this paper, three different excitation methods (harmonic, impulse, and Brownian drive) are applied to both cantilever (clamped-free beam) and bridge (clamped-clamped beam) type MEMS resonators which operate either in air or in a partial vacuum. In addition, each resonator is excited with electrostatic or piezo-crystal actuation at various temperatures. For each operation condition, resonant characteristics such as resonance frequency and Q-factor are extracted by appropriate nonlinear curve fittings. Therefore, effect of the actuation scheme, device type, vacuum level, and operating temperature on resonant characteristics of MEMS resonators can be thoroughly examined. To be more specific, we focus on measurement random uncertainties of resonant characteristics.

## 2. Experimental setup

Fig. 1 shows our experimental setup that is a homebuilt optical-lever setup. A polarized laser (Coherent, LabLaser ULN) of which diameter, wavelength, and power are 1 mm, 635 nm, and 5 mW, respectively, is expanded about five times with a

Table 1. Summary of the resonant characteristics of 4 silicon MEMS resonators at  $25^\circ\text{C}$ . 3 clamped-free beams (cantilevers) and 1 clamped-clamped beam (bridge) are used.

No.	Device type	Dimension ( $l \times w \times t$ )* [ $\mu\text{m}^3$ ]	Resonance frequency [kHz]	Q-Factor
#1	Cantilever 1	$406 \times 28.5 \times 12$	102.6903 ~102.6908	9,000 ~14,000
#2	Cantilever 2	$406 \times 28.5 \times 12$	101.9275 ~101.9278	600 ~800
#3	Cantilever 3	$110 \times 35 \times 1.0$	107.34 ~107.57	210 ~250
#4	Bridge	$748 \times 15.8 \times 12$	89.646 ~89.722	20,000 ~25,000

\*  $l$ : length,  $w$ : width, and  $t$ : thickness

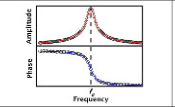
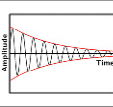
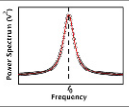
beam expander (Thorlabs, BE05M-A), goes through an iris, a polarizing beam splitter (Thorlabs, CM1-PBS251), a quarter wave plate (Thorlabs, WPQ10M-633), then is focused onto a MEMS resonator with a  $10\times$  microscope objective (Olympus, RMS10 $\times$  NA = 0.25). The reflected light travels back to the polarizing beam splitter and is focused onto a two-segmented photodetector. MEMS resonators are driven using a custom drive circuit in conjunction with a function generator (Agilent, 33250A) or a data acquisition card (National Instruments, NI-USB6361). The photodetector output is monitored with an oscilloscope (Agilent, DSO1012A) and recorded in a PC through the data acquisition card.

Four MEMS resonators are chosen in this work. Three of them are cantilevers and one of them is a bridge. Each resonator operates either in air or in a partial vacuum, thus allowing different device types and vacuum ranges to be examined. Resonant characteristics of each resonator are summarized in Table 1. In addition, each resonator directly attached to a temperature controllable mount can be excited electrostatically using integrated drive electrodes or acoustically using a piezo-crystal (Physik Instrumente GmbH PL033.30). Therefore, actuation and temperature effect on resonant characteristics and measurement uncertainties can be investigated.

## 3. Method

Three methods are applied to extract resonance frequency and Q-factor. Representative plots, equations, and general characteristics of the three methods exploited in this work are summarized in Table 2. The first method is called “*Frequency sweep (FS)*” where active drive signals are swept around the resonance frequency while the amplitude and phase responses from the resonator are measured. For the FS method, 1 output and 2 input channels of the NI data acquisition card are used in conjunction with the NI Sound and Vibration Toolkit™ to enable the frequency response function analysis. AC drive signals generated from the output channel which act as a reference are fed into one of the two analog inputs and measured photodetector signals are connected to the other analog input

Table 2. Comparison between three different methods to extract resonant characteristics (resonance frequency and Q-factor). The first method is called “Frequency Sweep (FS)” where the active drive signal is swept around the resonance frequency while the amplitude and phase responses from the resonator are measured in a lock-in configuration. The second method is called “Ring-down (RD)” where the decaying sinusoidal oscillation is monitored after a short-period active drive is applied. The third method is called “Thermal Noise (TN)” where the thermal noise spectrum of the resonator is measured without excitation. Data from each method are fitted with equations tabulated to extract resonance frequency and Q-factor.

	Active (driven) method		Passive (undriven) method
	Frequency Sweep (FS)	Ring-down (RD)	Thermal Noise (TN)
Representative Plots			
Equations	Eq. (1), (2), and (3)	Eq. (4)	Eq. (5)
Characteristics	<ul style="list-style-type: none"> <li>• Measurement time : 30–40 s/run</li> <li>• Active actuation is necessary.</li> <li>• Amplitude and phase data can be fitted individually or simultaneously.</li> </ul>	<ul style="list-style-type: none"> <li>• Measurement time : 0.1–1 ms/run</li> <li>• Active actuation is necessary.</li> <li>• Useful for devices having time drift.</li> </ul>	<ul style="list-style-type: none"> <li>• Measurement time : 1–40 min/run</li> <li>• No actuation is required.</li> <li>• Not suitable for devices having non-negligible time drift.</li> <li>• Significantly depends on noise characteristics of measurement system.</li> </ul>

channel. This is similar to a typical lock-in configuration and measurement. Maximum sampling rates of the NI-USB-6361 are  $2.86 \times 10^6$  samples/sec and  $2 \times 10^6$  samples/sec for analog output and input, respectively. Thus, the FS method is available for frequencies up to  $\sim 300$  kHz. For higher frequency range, combination of a function generator and an RF lock-in amplifier is recommended. Amplitude and phase data acquired are fitted independently using

$$X(f) = A_0 + \frac{F_0 f_n^2}{\sqrt{(f^2 - f_n^2)^2 + \frac{f^2 f_n^2}{Q^2}}} \quad (1)$$

$$\Phi(f) = A_1 - \arctan\left(\frac{f f_n}{Q(f^2 - f_n^2)}\right) \quad (2)$$

where  $f$  and  $f_n$  is drive frequency and resonance frequency,  $Q$  is Q-factor,  $A_0$ , and  $A_1$  are baseline offsets due to white noise, and  $F_0$  is the magnitude of the excitation (see Fig. 2(a)) [28, 29]. The electrostatic actuation is an external excitation and the piezo-crystal actuation is an inertial excitation. Though their excitation mechanisms are different, their equations of motion are the same considering the spring-mass-dashpot lumped parameter model and using absolute and relative coordinates for electrostatic and piezo-crystal actuations, respectively. Therefore, Eqs. (1) and (2) can be applied to both actuation methods. For electrostatic actuation, Eqs. (1) and (2) can be directly applied to extract resonance characteristics. For piezo-crystal actuation, however, nonlinear curve fittings often become problematic without baseline adjustment. Prior to nonlinear fittings, non-flat baselines likely due to parasitic couplings are corrected. If either Eq. (1) or (2) is used at a time, resonance frequency and Q-factor from each curve fit-

ting are not necessarily same. Fitted results from Eqs. (1) and (2) are denoted by FS\_A and FS\_P, respectively. Once both amplitude and phase are combined and expressed in a complex number format, nonlinear curve fitting using Eq. (3) results in a unique pair of resonance frequency and Q-factor (FS\_C, see Fig. 2(b)).

$$Z_R + iZ_I = X(f)\cos(\Phi) + iX(f)\sin(\Phi) \quad (3)$$

The second method is called “Ring-down (RD)” where the decaying sinusoidal oscillation is monitored after a short-period active drive is applied. Agilent function generator 33250A is operated in burst mode to provide a few cycles of sinusoidal drives once triggered. The number of cycles of the periodic drive necessary to saturate the amplitude response of a given resonator depends on the drive amplitude. In general, application of larger drive amplitudes requires smaller number of cycles. Once the burst drive stops, the resonator amplitude responses start to decay. A peak detection algorithm in a decaying sinusoid is employed to construct an envelope which is fitted using

$$X(t) = A_2 \quad (0 \leq t \leq t_0) \quad (4)$$

$$X(t) = A_2 e^{(-\pi f_n(t-t_0)/Q)} \quad (t > t_0)$$

where  $t_0$  is the time when the decay starts and  $A_2$  is the peak vibration amplitude before the burst drive stops [30, 31]. By adding  $t_0$  into the fitting equation, measurement random uncertainties are significantly reduced (see Fig. 2(c)).

The third method is called “Thermal noise (TN)” where thermal noise spectrum of the resonator is measured without excitation using the NI USB-6361. Due to the absence of active drive, thermal noise spectrum is weak, thus, requires averaging. In our measurements, five hundred spectra are averaged since results from the TN method start to converge around an averaging cycle of 500. Depending on the frequency span setting, such averaging could take up to 40 minutes. The current setup for acquiring thermal noise can be further improved by a high-end network or spectrum analyzer which exhibits better performance.

During thermal noise spectrum acquisition, a Fast Fourier Transform (FFT) algorithm with six different window functions (Blackman, Blackman-Harris, Exact Blackman, Hamming, Hanning, and None) is used. Acquired thermal noise spectra are fitted by

$$x^2(f) = A_3 + \frac{A_4}{Q \left[ \left( 1 - \left( \frac{f}{f_n} \right)^2 \right)^2 + \left( \frac{f}{f_n Q} \right)^2 \right]} \quad (5)$$

where  $A_3$  is a baseline due to white noise and  $A_4$  is a fitting parameter that combines temperature, stiffness, and Boltzmann’s constant [32] (see Fig. 2(d)). Generally, a window function is used to minimize spectral leakage during FFT [33].

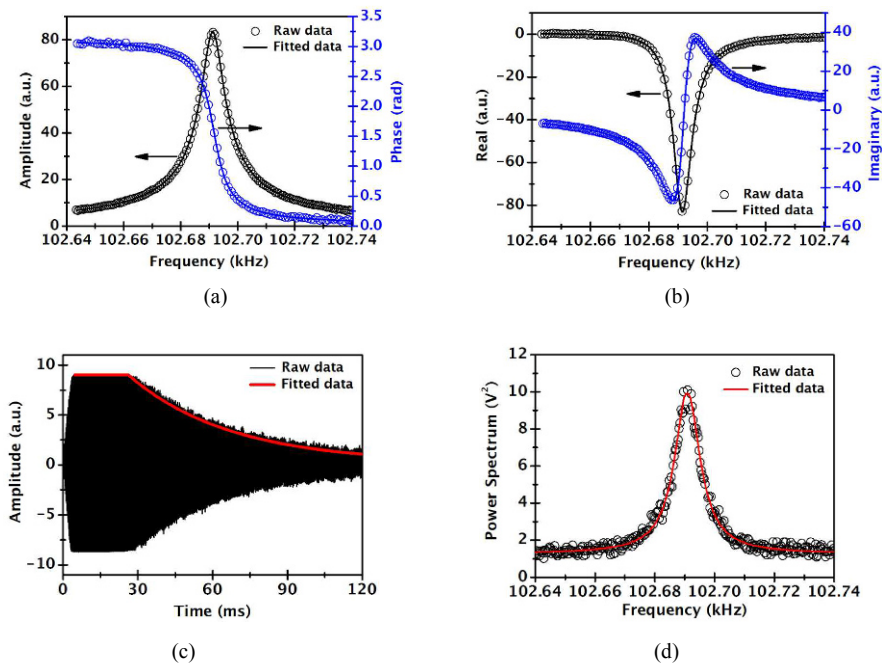


Fig. 2. Resonant characteristics of the cantilever 1(#1) measured with three different methods at 25°C. Electrostatic actuation is used for both the frequency sweep and ring-down methods. Resonance frequencies range from 102.6903 to 102.6908 kHz and Q-factors range from 13960 to 15417: (a) Either amplitude or phase information from the frequency sweep method is fitted (each fitting is designated with FS\_A and FS\_P, respectively); (b) Both amplitude and phase from the frequency sweep are fitted simultaneously (FS\_C); (c) Decaying sinusoidal oscillation is measured by sudden stop of the excitation signal and fitted (RD); (d) Without excitation, thermal noise spectrum of the same cantilever is taken and fitted (TN).

However, the FFT window function inevitably accompanies energy loss. As a result, extracted Q-factor using FFT tends to be smaller than the true Q-factor. Since the magnitude of such unwanted energy loss depends on the window function, it becomes a source of systematic uncertainty rather than random uncertainty. Depending on the window function chosen, the resulting Q-factor can vary up to ~8 % while the random uncertainty is insensitive to the window function in our measurements. In general, FFT without a window function (None) that exhibits Q-factor close to the average value from the six different window functions is used hereinafter. Although our main interest is to investigate measurement random uncertainties, systematic uncertainties can be also examined if the energy loss encountered during FFT is corrected as recently reported in Ref. [18].

## 4. Results and discussions

### 4.1 Actuation effect

First, cantilever 1 (#1) device is tested with both electrostatic and piezo-crystal actuation at 25°C to check whether measured resonant characteristics depend on actuation scheme. While electrostatic actuation causes dynamic displacement only within the free standing region of each resonator where a drive electrode is located, piezo-crystal actuation induces dynamic displacement within the whole chip where the piezo-crystal is mounted, including the clamped base and the free standing region. Fig. 3(a) shows normalized amplitude from

FS method with two actuation schemes. In general, normalized amplitude with electrostatic actuation is narrower than that with piezo-crystal actuation. For both actuation schemes, the peak shape of normalized amplitude (Full Width at Half Maximum : FWHM) is almost insensitive to the magnitude of driving force applied to each actuation scheme. Therefore, the observed trend can be thought to be actuation scheme dependent. In phase responses shown in Fig. 3(b), the electrostatic actuation exhibits much sharper transition from in-phase to out-of-phase near resonance frequency. This sharper phase transition is in line with the narrower FWHM. Results from FS method are fitted with Eqs. (1), (2), and (3) to extract resonance frequency and Q-factor.

Next, RD method with two actuation schemes is applied to #1 device and decaying oscillation responses are fitted with Eq. (4). To compare five curve fittings of our interest, TN method is also applied to #1 device and acquired thermal spectra are fitted with Eq. (5), although this is a passive method without active actuation. Fig. 3(c) and (d) show resonance frequencies and Q-factors from five different curve fittings. Data for TN method is shown in both top and bottom vignettes for comparison. General trends and nominal values of resonance frequency are independent of the actuation scheme. Active methods exhibit much lower random measurement uncertainties. In contrast, Q-factors obtained with piezo-crystal actuation are much lower than those with electrostatic actuation for both FS and RD methods. This is expected from the wider FWHM in amplitude responses with

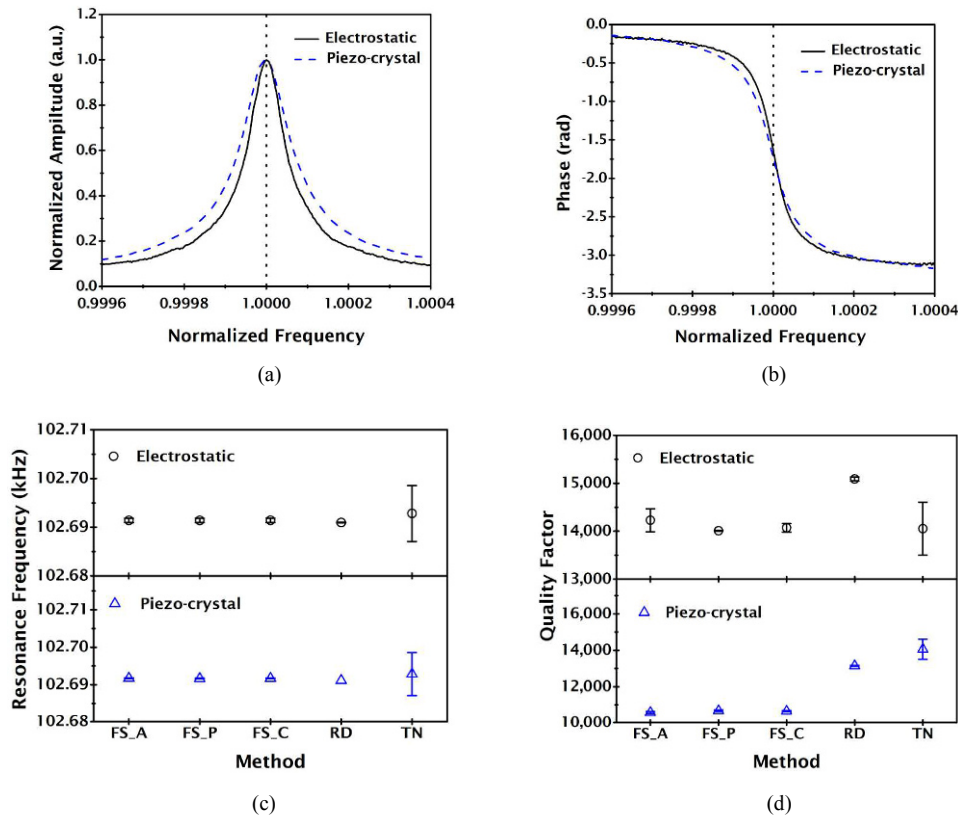


Fig. 3. Experimental comparison between electrostatic and piezo-crystal actuation using cantilever 1 (#1) at 25°C. Both drive schemes are applied to the frequency sweep and ring-down methods: (a) Normalized amplitude; (b) phase from the FS method. Full width at half maximum is narrower with electrostatic actuation than with piezo-crystal actuation; (c) Resonance frequencies; (d) Q-factors are extracted from corresponding curve fittings. Each error bar indicates the standard deviation ( $1\sigma$ ) from 5 consecutive measurements. General trends and nominal values of resonance frequency are independent of the actuation scheme. However, Q-factor obtained with piezo-crystal actuation is much lower than that with electrostatic actuation. In addition, the piezo-crystal actuation offers lower random uncertainty in both resonance frequency and Q-factor than the electrostatic actuation.

piezo-crystal actuation shown in Fig. 3(a). From our experiments, the piezo-crystal actuation seems to exhibit higher systematic uncertainty in Q-factor measurements than the electrostatic actuation, while it offers lower random uncertainty in both resonance frequency and Q-factor than the electrostatic actuation. Electrostatic actuation will be used hereafter except for cantilever 3 (#3) which does not have electrodes for electrostatic actuation.

#### 4.2 Device type effect

To examine the effect of device type on resonant characteristics, cantilever 1 (#1) and bridge (#4) are chosen. Of note, both devices have high Q-factors. Fig. 4 shows resonant characteristics measured with three different methods and five different curve fittings at 25°C. Resonance frequencies of #1 range from 102.690 to 102.692 kHz and Q-factors of #1 range from 13961 to 15417 (see Fig. 4(a) and (b)). Resonance frequencies of #4 range from 89.646 to 89.765 kHz and Q-factors of #4 range from 7302 to 22598 (see Fig. 4(c) and (d)). Regardless of device type, RD and TN methods exhibit the lowest and highest random measurement uncertainties, respec-

tively, in both resonance frequency and Q-factor. For #1, Q-factor from RD method is higher than that from other methods so it is possible that there is higher systematic uncertainty in RD method. For #4, Q-factor from TN method is much lower than that from other methods so it is likely that there is higher systematic uncertainty in TN method. This is due to the fact that #4 experiences appreciable time drift of resonance frequency for unknown reasons and TN method requires the longest measurement time among three methods. Though two extra bridge devices tested exhibit time drift similar to #4 (results not shown), we are not absolutely sure that every high Q-factor bridge resonator would have similar level of time drift. However, it is obvious that TN method is least preferred for resonators having non-negligible time drift.

#### 4.3 Vacuum level effect

Three cantilevers (#1, #2, and #3) are chosen to compare same type of resonators having different vacuum (or pressure) levels. All cantilevers have similar resonance frequencies around 100 kHz but quite different Q-factors since #1 and #2 are vacuum packaged with different quality and #3 is exposed

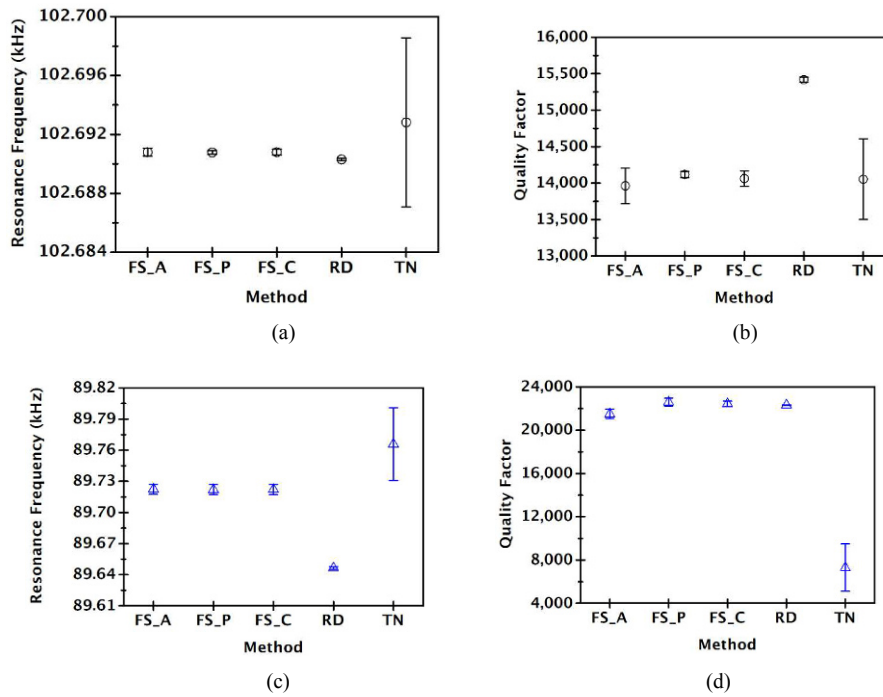


Fig. 4. Resonant characteristics of cantilever 1 (#1) and bridge (#4) measured with three different methods and five different curve fittings at 25°C. Electrostatic actuation is used for active methods: (a) Resonance frequencies of #1 range from 102.690 to 102.692 kHz; (b) Q-factors of #1 range from 13961 to 15417; (c) Resonance frequencies of #4 range from 89.646 to 89.765 kHz; (d) Q-factors of #4 range from 7302 to 22598. Each error bar indicates the standard deviation ( $1\sigma$ ) from 5 measurements. Regardless of device type, the RD and TN methods exhibit the smallest and largest random measurement uncertainties, respectively, in both resonance frequency and Q-factor. For #1, Q-factor from the RD method is higher than that from other methods so it is possible that there is larger systematic uncertainty in the RD method. For #4, Q-factor from the TN method is much lower than that from other methods so it is likely that there is larger systematic uncertainty in the TN method. This is due to the fact that #4 experiences appreciable temporal drift of resonance frequency for unknown reasons.

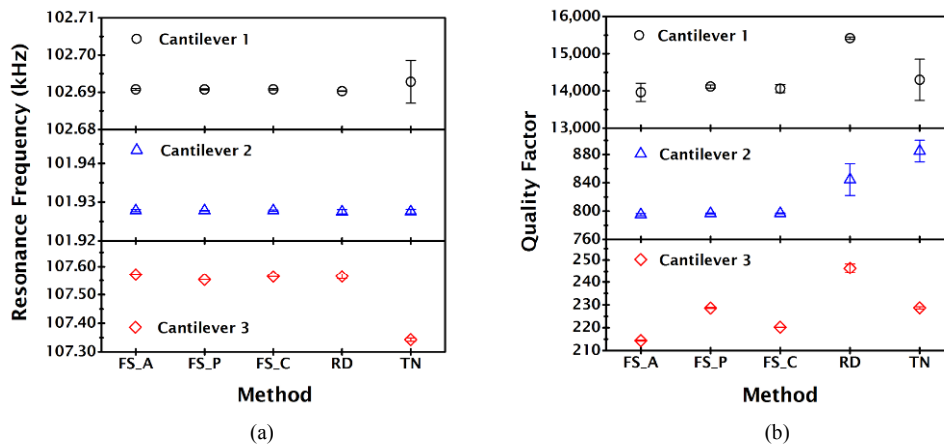


Fig. 5. Experimental comparison of three different cantilevers (#1, #2, and #3) operating either in air or in a partial vacuum. #1 and #2 are vacuum packaged but the quality of the vacuum packaging is different and #3 is exposed to ambient air (atmospheric pressure). All cantilevers have similar resonance frequencies around 100 kHz but quite different Q-factors. (a) Resonance frequencies of #1, #2, and #3 are 102.6903~102.6939, 101.9275~101.9278, and 107.3428~107.5716 kHz, respectively. (b) Q-factors of #1, #2, and #3 are 13962~15418, 795~885, and 214~246, respectively. Each error bar indicates the standard deviation ( $1\sigma$ ) from 5 consecutive measurements.

to air. Fig. 5 shows resonant characteristics for three cantilevers chosen with three different methods and five different curve fittings at 25°C. Resonance frequencies of #1, #2, and #3 are 102.6903~102.6939, 101.9275~101.9278, and 107.3428~107.5716 kHz, respectively (see Fig. 5(a)). Q-factors of #1, #2, and #3 are 13962~15418, 795~885, and

214~246, respectively (see Fig. 5(b)). Vacuum packaged devices (#1 and #2) exhibit lower systematic uncertainties in resonance frequency than the device operating at atmospheric pressure (#3). TN method results in much lower random uncertainties in Q-factor for #3 than those for #1 and #2 while it provides lower resonance frequency than other methods and

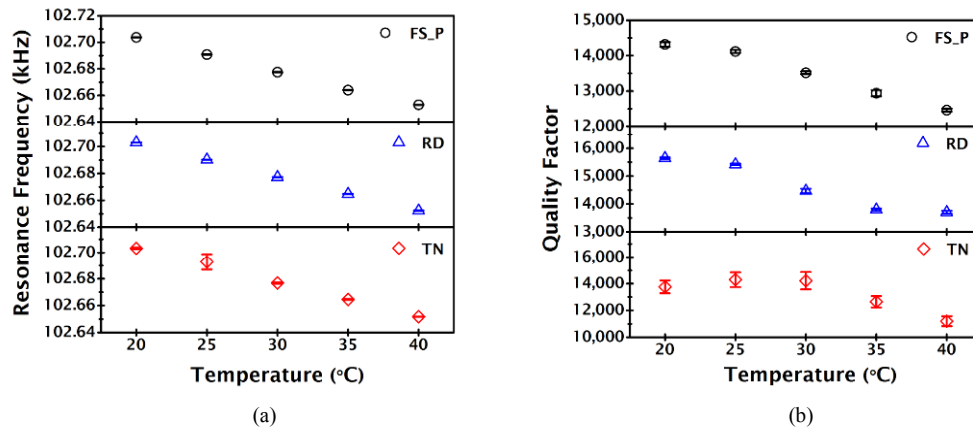


Fig. 6. (a) Resonance frequencies and (b) Q-factors of cantilever 1 (#1) measured with three different methods/curve fittings (FS\_P, RD, and TN) at five different temperatures (20, 25, 30, 35, and 40°C) are compared. Each error bar indicates the standard deviation ( $1\sigma$ ) from 5 consecutive measurements. In general, both resonance frequency and Q-factor decrease as temperature increases. Temperature coefficients of the resonance frequency are 25.1, 24.8, and 24.9 ppm/°C for FS\_P, RD, and TN methods, respectively. Resonance frequencies extracted are insensitive to the method applied while Q-factors are method-dependent. Among three methods, RD method provides the highest Q-factor and TN method exhibits the highest random measurement uncertainties in both resonance frequency and Q-factor.

curve fittings for #3. In general, RD method results in higher Q-factor than FS method. RD method, however, results in higher Q-factor than TN method for #1 and #3 and lower Q-factor than TN method for #2. Both quantitative and qualitative comparison in systematic and random uncertainties observed in different methods and curve fittings is possibly dependent on operating/damping conditions.

#### 4.4 Temperature effect

Resonance frequency of silicon MEMS resonators tends to decrease with increasing temperature since elastic modulus of silicon decreases [34]. Since resonance frequency is less sensitive to methods/curve fittings than Q-factor, temperature dependent resonance frequency change is not likely to be sensitive to methods/curve fittings. However, it is not crystal clear whether heating is favorable to damping and whether temperature dependent Q-factor change is similar for different methods/curve fittings. To clarify these, resonance frequency and Q-factor of cantilever 1 (#1) are measured with three different methods at five different temperatures (20, 25, 30, 35, and 40°C). Since results from FS method with three different fittings are similar and indistinguishable when plotted together, results from FS\_P, RD, and TN are shown in Fig. 6. In general, both resonance frequency and Q-factor decrease as temperature increases. Temperature coefficients of the resonance frequency are 25.1, 24.8, and 24.9 ppm/°C for FS\_P, RD, and TN methods, respectively. As expected, resonance frequencies extracted are insensitive to the method applied while Q-factors are method-dependent. As temperature increases, Q-factors from FS and RD methods decrease monotonically and Q-factors from TN are somewhat insensitive to temperature below 30°C and decrease beyond that. This is possibly due to the fact that TN method requires longer time for each run than

other methods. Among three methods, RD method provides the highest Q-factor and TN method exhibits the highest random measurement uncertainties in both resonance frequency and Q-factor. Table 3 summarizes fitting parameters and R-squared values for each operating conditions investigated and fitting schemes employed in this work.

#### 5. Conclusions

To quantify measurement uncertainties in resonance frequency and Q-factor of MEMS resonators, and to investigate various parameters which affect resonant characteristics, three different methods and five nonlinear curve fittings are applied to both cantilever and bridge resonators which operate either in air or in a partial vacuum. In addition, each resonator is excited with electrostatic or piezo-crystal actuation at various temperatures. To summarize, piezo-crystal actuation results in higher systematic uncertainty and lower random uncertainty in Q-factor measurement than electrostatic actuation. Measured resonance frequencies are almost independent of the actuation scheme applied. Active and passive methods do not provide identical results in both resonance frequency and Q-factor. Measured resonance frequency and Q-factor even depend on the active method (frequency sweep or ring-down) used and the nonlinear curve fitting chosen. In general, frequency sweep method with phase fitting is recommended since it provides the lowest random uncertainty and the highest fitting quality as summarized in Table 3. For resonators having non-negligible time drift of resonance frequency, TN method is not recommended. General trends and magnitude comparisons of resonance frequency and Q-factor from different curve fittings change depending on the surrounding pressure. For three different methods, resonance frequency linearly decreases with temperature, and temperature coefficients of resonance fre-

Table 3. Summary of fitting parameters and R-squared values for each operating condition and fitting function. Actuation is applied to FS and RD methods only.

Device and condition	Methods	$f$ [Hz]	$\sigma_f$ [Hz]	$Q$	$\sigma_Q$	$R^2$
#1 at 25°C (electrostatic actuation)	FS_A	102691.4	0.43	14228.93	240.37	0.99912
	FS_P	102691.4	0.43	14009.66	10.30	0.99993
	FC_C	102691.4	0.43	14072.21	88.78	0.99946
	RD	102691.0	0.09	15088.36	42.11	0.99298
	TN	102692.8	5.75	14053.91	552.94	0.94695
#2 at 25°C (electrostatic actuation)	FS_A	101927.8	0.25	795.21	1.51	0.99992
	FS_P	101927.8	0.13	796.65	0.70	0.99997
	FC_C	101927.8	0.17	796.77	0.49	0.99995
	RD	101927.5	0.54	844.55	22.30	0.98191
	TN	101927.5	0.57	884.98	15.17	0.98342
#3 at 25°C (electrostatic actuation)	FS_A	107571.6	0.24	214.37	0.16	0.99937
	FS_P	107553.4	0.13	228.59	0.16	0.99971
	FC_C	107564.5	0.10	220.21	0.05	0.99947
	RD	107565.1	7.86	246.35	1.97	0.98726
	TN	107342.8	5.76	228.72	0.51	0.87043
#4 at 25°C (electrostatic actuation)	FS_A	89722.38	4.88	21510.58	412.95	0.99774
	FS_P	89722.06	4.88	22598.23	364.36	0.99956
	FC_C	89722.19	4.88	22431.27	246.92	0.99584
	RD	89646.45	1.36	22315.82	31.09	0.98965
	TN	89765.88	34.93	7302.81	2188.07	0.88945
#1 at 20°C (electrostatic actuation)	FS_A	102703.8	0.12	14098.88	221.30	0.99943
	FS_P	102703.7	0.11	14316.99	67.30	0.99984
	FC_C	102703.8	0.11	14238.70	97.97	0.99956
	RD	102703.0	0.11	15639.70	31.28	0.99842
	TN	102703.2	0.51	13760.24	482.75	0.97012
#1 at 30°C (electrostatic actuation)	FS_A	102677.5	0.15	13559.79	205.70	0.99947
	FS_P	102677.5	0.12	13515.08	39.51	0.99992
	FC_C	102677.5	0.13	13521.53	74.99	0.99963
	RD	102677.3	0.10	14469.77	76.56	0.99811
	TN	102676.8	0.49	14771.05	651.89	0.95034
#1 at 35°C (electrostatic actuation)	FS_A	102664.0	0.16	12892.04	301.64	0.99883
	FS_P	102664.0	0.09	12939.76	89.19	0.99976
	FC_C	102664.0	0.12	12917.37	124.45	0.99924
	RD	102664.7	0.07	13797.35	42.30	0.99640
	TN	102664.5	0.45	12644.63	420.79	0.98302
#1 at 40°C (electrostatic actuation)	FS_A	102653.0	0.17	12122.19	437.93	0.99924
	FS_P	102652.9	0.14	12460.21	39.89	0.99989
	FC_C	102653.0	0.14	12353.75	130.51	0.99944
	RD	102652.3	0.12	13704.22	51.48	0.99347
	TN	102651.7	0.16	11193.06	368.91	0.99072
#1 at 25°C (piezo-crystal actuation)	FS_A	102691.7	0.09	10574.37	52.84	0.99973
	FS_P	102691.6	0.11	10672.17	44.31	0.99995
	FC_C	102691.7	0.10	10644.23	32.11	0.99984
	RD	102691.1	0.00	13140.89	30.83	0.99729
	TN	102692.8	5.75	14053.91	552.94	0.94695

quency are almost similar. Q-factor, however, may not vary always in a monotonic fashion as temperature increases.

Our results suggest a better method for precision measurements of resonance frequency and Q-factor for some situations and recommend specifying experimental conditions including the actuation scheme when reporting resonant characteristics of mechanical resonators.

## Acknowledgment

This research was supported by Basic Science Research Program through the National Research Foundation of Korea (NRF) funded by the Ministry of Education, Science and Technology (2011-0012942).



## References

- [1] A. N. Cleland and M. L. Roukes, A nanometre-scale mechanical electrometer, *Nature*, 392 (1998) 160-162.
- [2] W. Pang, H. Y. Yu, H. Zhang and E. S. Kim, Temperature-compensated film bulk acoustic resonator above 2 GHz, *IEEE Electron Device Lett.*, 26 (2005) 369-371.
- [3] I. D. Avramov, Gigahertz range resonant devices for oscillator applications using shear horizontal acoustic-waves, *IEEE Trans. Ultrason. Ferroelectr. Freq. Control*, 40 (1993) 459-468.
- [4] S. Hur, S. Q. Lee and H. S. Choi, Fabrication and characterization of PMN-PT single crystal cantilever array for cochlear-like acoustic sensor, *J. Mech. Sci. Technol.*, 24 (2010) 181-184.
- [5] K. J. Coakley, J. D. Splett, M. D. Janezic and R. F. Kaiser, Estimation of Q-factors and resonant frequencies, *IEEE Trans. Microw. Theory Tech.*, 51 (2003) 862-868.
- [6] W. H. Han, S. M. Lindsay and T. W. Jing, A magnetically driven oscillating probe microscope for operation in liquids, *Appl. Phys. Lett.*, 69 (1996) 4111-4113.
- [7] X. P. Feng, Theory of a short optical cavity with dielectric multilayer film mirrors, *Opt. Commun.*, 83 (1991) 162-176.
- [8] S. Ohteru and N. Takachio, Optical signal quality monitor using direct Q-factor measurement, *IEEE Photonics Technol. Lett.*, 11 (1999) 1307-1309.
- [9] S. Wozniak, Resonant optical rectification in chiral molecular systems: Application to a three-level model, *Acta Phys. Pol. A*, 90 (1996) 519-522.
- [10] J. W. Lee, Analysis of fluid-structure interaction for predicting resonant frequencies and quality factors of a microcantilever on a squeeze-film, *J. Mech. Sci. Technol.*, 25 (2011) 3005-3013.
- [11] S. Prescesky, M. Parameswaran, A. Rawicz, R. F. B. Turner and U. Reichl, Silicon micromachining technology for subnanogram discrete mass resonant biosensors, *Can. J. Phys.*, 70 (1992) 1178-1183.
- [12] T. Ono and M. Esashi, Mass sensing with resonating ultrathin silicon beams detected by a double-beam laser Doppler vibrometer, *Meas. Sci. Technol.*, 15 (2004) 1977-1981.
- [13] W. Y. Shih, X. P. Li, H. M. Gu, W. H. Shih and I. A. Aksay, Simultaneous liquid viscosity and density determination with piezoelectric unimorph cantilevers, *J. Appl. Phys.*, 89 (2001) 1497-1505.
- [14] R. Patois, P. Vairac and B. Cretin, Near-field acoustic densimeter and viscosimeter, *Rev. Sci. Instrum.*, 71 (2000) 3860-3863.
- [15] F. R. Blom, S. Bouwstra, M. Elwenspoek and J. H. J. Fluitman, Dependence of the quality factor of micromachined silicon beam resonators on pressure and geometry, *J. Vac. Sci. Technol. B*, 10 (1992) 19-26.
- [16] F. H. Lei, J. F. Angiboust, W. Qiao, G. D. Sockalingum, S. Dukic, L. Chrit, M. Troyon and M. Manfait, Shear force near-field optical microscope based on Q-controlled bimorph sensor for biological imaging in liquid, *J. Microsc.* 216 (2004) 229-233.
- [17] S. Rast, C. Wattinger, U. Gysin and E. Meyer, The noise of cantilevers, *Nanotechnology*, 11 (2000) 169-172.
- [18] J. E. Sader, J. Sanelli, B. D. Hughes, J. P. Monty and E. J. Bieske, Distortion in the thermal noise spectrum and quality factor of nanomechanical devices due to finite frequency resolution with applications to the atomic force microscope, *Rev. Sci. Instrum.*, 82 (2011) 095104.
- [19] S. Miller, K. Turner and N. MacDonald, Microelectromechanical scanning probe instruments for array architectures, *Rev. Sci. Instrum.*, 68 (1997) 4155-4162.
- [20] J. Brugger, N. Blanc, P. Renaud and N. De Rooij, Microlever with combined integrated sensor/actuator functions for scanning force microscopy, *Sens. Actuator A-Phys.*, 43 (1994) 339-345.
- [21] M. Cunningham, D. Jenkins, W. Clegg and M. Bakush, Active vibration control and actuation of a small cantilever for applications in scanning probe instruments, *Sens. Actuator A-Phys.*, 50 (1995) 147-150.
- [22] J. Lee and W. King, Microcantilever actuation via periodic internal heating, *Rev. Sci. Instrum.*, 78 (2007) 126102.
- [23] D. Rugar and P. Grutter, Mechanical parametric amplification and thermomechanical noise squeezing, *Phys. Rev. Lett.*, 67 (1991) 699-702.
- [24] J. Davis, D. Vick, D. Fortin, J. Burgess, W. Hiebert and M. Freeman, Nanotorsional resonator torque magnetometry, *Appl. Phys. Lett.*, 96 (2010) 072513.
- [25] K. Y. Yasumura, T. D. Stowe, E. M. Chow, T. Pfafman, T. W. Kenny, B. C. Stipe and D. Rugar, Quality factors in micron- and submicron-thick cantilevers, *J. Microelectromech. Syst.*, 9 (2000) 117-125.
- [26] J. Q. Han, C. C. Zhu, J. H. Liu and P. Li, A novel temperature-compensating structure for micromechanical bridge resonator, *J. Micromech. Microeng.*, 15 (2005) 702-705.
- [27] X. Xu and A. Raman, Comparative dynamics of magnetically, acoustically, and Brownian motion driven microcantilevers in liquids, *J. Appl. Phys.*, 102 (2007) 034303.
- [28] J. H. Seo, Silicon-based resonant microsensor platform for chemical and biological applications, *PhD Dissertation*, School of Electrical and Computer Engineering, Georgia Institute of Technology (2007).
- [29] K. Naeli and O. Brand, An iterative curve fitting method for accurate calculation of quality factors in resonators, *Rev. Sci. Instrum.*, 80 (2009) 045105.
- [30] A. R. Klempner, R. T. Marinis, P. Hefti and R. J. Pryputniewicz, Experimental determination of the Q-factors of microcantilevers coated with thin metal films, *Strain*, 45 (2009) 295-300.
- [31] S. S. Verbridge, H. G. Craighead and J. M. Parpia, A megahertz nanomechanical resonator with room temperature quality factor over a million, *Appl. Phys. Lett.*, 92 (2008) 013112.
- [32] G. A. Matei, E. J. Thoreson, J. R. Pratt, D. B. Newell and N. A. Burnham, Precision and accuracy of thermal calibration of atomic force microscopy cantilevers, *Rev. Sci. Instrum.*,

77 (2006) 083703.

- [33] F. J. Harris, On the use of windows for harmonic analysis with the discrete Fourier transform, *Proceedings of the IEEE*, 66 (1978) 51-83.
- [34] J. Lee, F. Goericke and W. King, Temperature-dependent thermomechanical noise spectra of doped silicon microcantilevers, *Sens. Actuator A-Phys.*, 145 (2008) 37-43.



**Il Lee** received his B.S. degree from the Department of Mechanical Engineering at Sogang University in 2012. He is currently working towards his M.S. in the Department of Mechanical Engineering at Sogang University. His research interests include MEMS fabrication and characterization.



**Jungchul Lee** received his B.S. and M.S. degrees in the Department of Mechanical Engineering from Seoul National University, Seoul, Korea in 2001 and 2003, respectively. He received his Ph.D. degree from the Georgia Institute of Technology in 2007. His dissertation was "Fabrication, Characterization, and

Application of Multifunctional Microcantilever Heaters." During 2007-2008, he worked as a postdoctoral research associate in mechanical science and engineering at the University of Illinois Urbana-Champaign. After spending 2 years (2008-2010) in the Department of Biological Engineering at the Massachusetts Institute of Technology as a postdoctoral research associate, he is now on the faculty in the Department of Mechanical Engineering at Sogang University, Seoul, Korea.